

# Achievable Sum Rate Optimization on NOMA-aided Cell-Free Massive MIMO with Finite Blocklength Coding

Baolin Chong, Hancheng Lu, *Senior Member, IEEE*, Yang Chen, Langtian Qin  
and Fengqian Guo

## Abstract

Non-orthogonal multiple access (NOMA)-aided cell-free massive multiple-input multiple-output (CFmMIMO) has been considered as a promising technology to fulfill strict quality of service requirements for ultra-reliable low-latency communications (URLLC). However, finite blocklength coding (FBC) in URLLC makes it challenging to achieve the optimal performance in the NOMA-aided CFmMIMO system. In this paper, we investigate the performance of the NOMA-aided CFmMIMO system with FBC in terms of achievable sum rate (ASR). Firstly, we derive a lower bound (LB) on the ergodic data rate. Then, we formulate an ASR maximization problem by jointly considering power allocation and user equipment (UE) clustering. To tackle such an intractable problem, we decompose it into two sub-problems, i.e., the power allocation problem and the UE clustering problem. A successive convex approximation (SCA) algorithm is proposed to solve the power allocation problem by transforming it into a series of geometric programming problems. Meanwhile, two algorithms based on graph theory are proposed to solve the UE clustering problem by identifying negative loops. Finally, alternative optimization is performed to find the maximum ASR of the NOMA-aided CFmMIMO system with FBC. The simulation results demonstrate that the proposed algorithms significantly outperform the benchmark algorithms in terms of ASR under various scenarios.

## Index Terms

Baolin Chong, Hancheng Lu, Yang Chen, Langtian Qin and Fengqian Guo are with the Department of Electronic Engineering and Information Science, University of Science and Technology of China, Hefei 230027, China. (e-mail: chongbaolin@mail.ustc.edu.cn; hclu@ustc.edu.cn; yangchen21@mail.ustc.edu.cn; qlt315@mail@mail.ustc.edu.cn; fqguo@ustc.edu.cn)

Cell-free massive multiple-input multiple-output (CFmMIMO), non-orthogonal multiple access (NOMA), ultra-reliable low-latency communication (URLLC), finite blocklength coding (FBC), graph theory.

## I. INTRODUCTION

ULTRA-reliable low-latency communications (URLLC) is an emerging communication technology that has garnered significant research attention due to its vast potential in supporting applications such as virtual reality (VR) and augmented reality (AR), haptic internet, vehicle networks, and autonomous systems [1]–[3]. Unlike other communication technologies, URLLC imposes stringent quality of service (QoS) requirements in terms of latency and reliability on the communication process [4]–[6]. For example, URLLC communication services typically require a target reliability of  $1-10^{-5}$  within 1 ms user plane latency, according to Third Generation Partnership Project (3GPP) standards [7]. Hence, URLLC brings huge pressure on wireless communication systems. Particularly, the edge effect of traditional cellular-based wireless communication systems, i.e., edge users suffering from severe signal interference and low achievable rate, will become a major obstacle to implement URLLC.

Non-orthogonal multiple access (NOMA)-aided cell-free massive multiple-input multiple-output (CFmMIMO) has been considered as a promising 6G technology to fulfill strict QoS requirements for URLLC. CFmMIMO is a combination of massive multiple-input multiple-output (MIMO) and distributed MIMO, which employs a CPU to control multiple access points (APs) to concurrently serve multiple user equipments (UEs) on the same time-frequency resources [8], [9]. The distributed deployment of APs greatly reduces the large-scale fading between UEs and APs [10], resulting in significant improvements in spectral efficiency (SE) [8] and energy efficiency (EE) [11] to support URLLC. Furthermore, due to the fact that all UEs are served simultaneously by all APs, the traditional cell boundaries disappear, eliminating the edge effect and making it possible to implement URLLC. However, since all UEs use the same time-frequency resources, UEs in CFmMIMO suffer severe interference from other UEs. To address this issue, NOMA technology is introduced into CFmMIMO to replace orthogonal multiple access [12]. In the downlink (DL) NOMA-aided CFmMIMO system, UEs transmit or receive signals at different power levels. Specifically, in the same time-frequency resource, successive interference cancellation (SIC) technology is used to enable UEs with better channel conditions and lower allocated power to cancel the interference caused by UEs with worse channel conditions and higher allocated power.

Many research attempts have been made on performance analysis and optimization of NOMA-aided CFmMIMO systems, especially in terms of achievable sum rate (ASR). [12] and [13] derived the ASR in the DL and uplink (UL) NOMA-aided CFmMIMO system, respectively. In [14], the author further derived the DL ASR and a closed-form expression for the signal-to-interference noise ratio (SINR) over spatially correlated Rician fading channels, while [15] considered the system under channel non-reciprocity. The authors of [16] focused on investigating the impact of different precoder schemes on system performance. Stochastic geometry approaches were also used to more realistically simulate wireless channel transmission characteristics more realistically in [17] and [18], investigating achievable rates. The author of [19] derived the DL SE and EE for Internet of Things (IoT) over spatially correlated Rician fading channels. Additionally, there are several works dedicated to optimizing the performance of the NOMA-aided CFmMIMO system. [13] and [19] consider power control during UL data transmission to maximize the minimum achievable rate and sum SE, respectively. Two power allocation algorithms are proposed in [20] and [21] for DL data transmission to maximize the minimum SE and sum SE, respectively. The author of [21] and [22] have centered their research on UE clustering within the system, proposing a sophisticated mechanism that utilizes the K-means algorithm, as well as an algorithm that maximizes the minimum DL rate, thereby achieving optimal performance.

Aforementioned work has proved that NOMA-aided CFmMIMO can significantly enhance the performance of wireless communication systems to support URLLC. However, for URLLC, the performance analysis and optimization on NOMA-aided CFmMIMO systems should be reconsidered. To ensure low latency and simplify the decoding complexity at the receiver, short packets are used for data transmission in URLLC [23]–[25]. In this case, the Shannon formula, which is based on the law of large numbers, is no longer applicable due to the non-negligible decoding error probability caused by finite blocklength coding (FBC). In [23], an approximate expression for the maximum achievable rate with respect to decoding error probability, code length, and signal-to-noise ratio (SNR) under FBC has been derived. Unlike the Shannon formula, the maximum achievable rate under FBC is neither convex nor concave with respect to SNR [26]. Existing work on performance analysis and optimization of NOMA-aided CFmMIMO systems are no longer applicable when considering URLLC.

In this paper, we theoretically analyze the impact of FBC on the NOMA-aided CFmMIMO system and attempt to achieve the optimal performance in terms of ASR by jointly optimizing

power allocation and UE clustering. To the best of our knowledge, this is the first study on NOMA-aided CFmMIMO system for URLLC. The main contributions of this paper are summarized as follows:

- We propose a NOMA-aided CFmMIMO system with consideration of URLLC, where all APs serve URLLC UEs in different clusters simultaneously. Then, we analyze the system performance and derive the lower bound (LB) for the ergodic data rate of URLLC UEs under FBC. To optimize the system performance, we formulate the ASR maximization problem by jointly considering the power allocation and UE clustering. To tackle such an intractable problem, we decompose it into two sub-problems, i.e., the power allocation problem and the UE clustering matrix design problem. By doing so, the original problem can be efficiently solved by a two-step iterative optimization algorithm.
- We use successive convex approximation (SCA) to solve the power allocation problem. Specifically, the objective function (OF) is first transformed into a convex function using logarithmic transformation. Then, the complex constraint conditions generated during the transformation process are converted into convex constraints through scaling. By utilizing SCA, the original power control problem is transformed into a series of geometric programming (GP) problems that can be solved efficiently.
- We solve the UE clustering matrix design problem based on graph theory. Specifically, we first reformulate the UE clustering problem as a negative loop detection problem in a weight directed graph. Then, we construct a weight directed graph based on the current clustering situation. Finally, we adopt two negative loop searching algorithms to effectively find the negative loops in the graph.

Simulation results validate the tightness of the derived LB, and demonstrate that the proposed algorithms outperform the benchmark algorithms in terms of the ASR under various scenarios.

The rest of the paper is organized as follows. Section II gives the DL NOMA-aided CFmMIMO system model and formulate the joint power allocation and UE clustering problem for maximizing the ASR. An iterative optimization algorithm is proposed in Section III, where the power allocation problem is transformed into a series of GP problems and the UE clustering matrix design problem is converted into the problem of finding *differ-cluster negative loop* based on graph theory. Section IV presents the evaluation results and analysis. Finally, the conclusion is drawn in Section V.

*Notations:* In this paper, vectors and matrices are denoted by lowercase and uppercase bold

TABLE I  
LIST OF KEY NOTATIONS

Symbol	Description
$M, N, G$	Number of APs, URLLC UEs and clusters
$L$	Number of antennas each AP
$\mathbf{X}, \boldsymbol{\pi}$	UE cluster matrix and vector
$\mathbf{h}_{mn}, \hat{\mathbf{h}}_{mn}$	Actual and estimated channel between AP $m$ and URLLC UE $n$
$p_p, n_p$	Pilot power and the length of pilot signal
$n_d$	Coding blocklength during DL transmission
$\mathbf{w}_{m\pi_n}$	Beamforming vector
$R_n$	Actual ergodic data rate of URLLC UE $n$
$\hat{R}_n$	LB of ergodic data rate for URLLC UE $n$
$p_n$	Transmit power that allocated to URLLC UE $n$
$\theta_{mn}$	Coefficient of estimated channel between AP $m$ and URLLC UE $n$
$\beta_{mn}$	Large-scale fading between AP $m$ and URLLC UE $n$
$c_n$	Imperfect SIC coefficient of URLLC UE $n$
$\gamma_n$	SINR of URLLC UE $n$
$p_{max}$	Maximum transmit power each AP
$\hat{R}_n^{req}$	Minimum rate requirement for URLLC UE $n$

letters, respectively.  $x_{i,j}$  represents the  $i$ -th row and  $j$ -th column element of matrix  $\mathbf{X}$  and  $\mathbf{X}^H$  represent the Hermitian of  $\mathbf{X}$ .  $\pi_i$  denotes the  $i$ -th elements of vector  $\boldsymbol{\pi}$ .  $\mathbb{C}^{i \times j}$  represents space of  $i \times j$  complex number matrices.  $\mathbb{E}[i]$  denotes the expected value of  $i$ .

## II. SYSTEM MODEL AND PROBLEM FORMATION

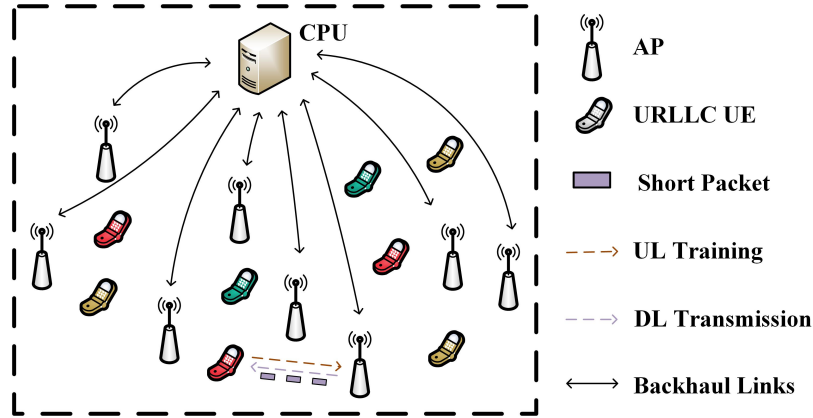


Fig. 1. The NOMA-aided CFmMIMO system for URLLC.

Consider a DL transmission scenario in a NOMA-aided CFmMIMO system, where a group of

$N$  URLLC UEs, each equipped with a single antenna, are served by  $M$  APs that are equipped with  $L$  antennas each, as illustrated in Fig. 1. In the figure, different clusters, represented by different colors, are formed, with each cluster containing a subset of URLLC UEs. Within each cluster, NOMA is employed, while orthogonal multiple access is utilized across different clusters. To represent the association between URLLC UEs and clusters, we employ a matrix  $\mathbf{X} \in \mathbb{C}^{G \times N}$  and a vector  $\boldsymbol{\pi} \in \mathbb{C}^{N \times 1}$ . Specifically, if URLLC UE  $n$  is allocated to cluster  $g$ , then  $x_{gn} = 1$  and  $\pi_n = g$ ; otherwise  $x_{gn} = 0$ . Note that different UE clustering matrices can have diverse impacts on the system's performance.

The channel model is assumed as Rayleigh fading channel, where the channel between AP  $m$  and URLLC UE  $n$  is represented as  $\mathbf{h}_{mn} = \sqrt{\beta_{mn}}\boldsymbol{\zeta}_{mn}$ . Here,  $\beta_{mn}$  represents the large-scale fading coefficient influenced by path loss and shadow fading. The small-scale fading vector  $\boldsymbol{\zeta}_{mn} \in \mathbb{C}^{L \times 1}$  consists of i.i.d. complex Gaussian random variables with zero mean and unit variance, i.e.,  $\mathcal{CN}(0, 1)$ . Table I lists a compilation of the main notations used in this paper.

#### A. UL Pilot Training and Channel Estimation

In order to estimate the instantaneous channel state information (CSI) for beamforming, all URLLC UEs simultaneously transmit pilot signals to all APs in the pre-transmission phase. Within the same cluster, URLLC UEs share a common pilot signal, while pilot signals are orthogonal between different clusters, thereby reducing the length of the pilot signal to  $G$ . Specifically, the pilot sequence transmitted by cluster  $g$  is denoted by  $\boldsymbol{\phi}_g \in \mathbb{C}^{n_p \times 1}$ , where  $n_p$  represents the length of the pilot signal and  $\|\boldsymbol{\phi}_g\|^2 = 1$ . However, it holds that  $\boldsymbol{\phi}_g^H \boldsymbol{\phi}_{g'} = 0, \forall g \neq g'$  for different clusters  $g$  and  $g'$  due to orthogonality. The received signal at AP  $m$  is given by  $\mathbf{Y}_m^p = \sqrt{n_p p_p} \sum_{n=1}^N \sum_{g=1}^G x_{gn} \mathbf{h}_{mn} \boldsymbol{\phi}_g^H + \mathbf{N}_m$ , where  $p_p$  denotes the pilot transmit power, and  $\mathbf{N}_m \in \mathbb{C}^{L \times n_p}$  is a Gaussian noise matrix with i.i.d  $\mathcal{CN}(0, 1)$  elements. After receiving the signals, all APs estimate instantaneous CSI with all URLLC UEs after receiving signal using minimum mean square error (MMSE) estimation. The MMSE estimate of  $\mathbf{h}_{mn}$  can then be expressed as  $\hat{\mathbf{h}}_{mn} = \frac{\sqrt{n_p p_p} \beta_{mn}}{1 + n_p p_p \sum_{n'=1}^N x_{\pi_n n'} \beta_{mn'}}$   $\mathbf{y}_{m\pi_n}^p$ . Since the received pilot signal  $\mathbf{y}_{m\pi_n}^p$  follows a Gaussian distribution [16], the MMSE estimate  $\hat{\mathbf{h}}_{mn}$  can be reexpressed as

$$\hat{\mathbf{h}}_{mn} = \sqrt{\theta_{mn}} \boldsymbol{\nu}_{m\pi_n}, \quad (1)$$

where the coefficient  $\theta_{mn}$  is given by  $\theta_{mn} = \frac{n_p p_p \beta_{mn}^2}{1 + n_p p_p \sum_{n'=1}^N x_{\pi_n n'} \beta_{mn'}}$  and is influenced by the UE clustering matrix  $\mathbf{X}$ . Here,  $\boldsymbol{\nu}_{m\pi_n} \sim \mathcal{CN}(0, \mathbf{I}_L)$  represents a circularly symmetric complex

Gaussian random vector with zero mean and identity covariance matrix.

### B. DL Data Transmission

DL data transmission can be achieved based on UL pilot training. The CPU receives instantaneous CSI estimates from all APs, enabling it to determine power allocation and UE clustering matrix. Subsequently, all APs perform beamforming and transmit signals to all URLLC UEs. The signal transmitted from AP  $m$  is represented as  $\mathbf{x}_m = \sum_{n=1}^N \sqrt{p_n} \mathbf{w}_{m\pi_n} q_n$ , where  $q_n$  and  $p_n$  denote the data signal and the transmit power allocated to URLLC UE  $n$ , respectively. The spatial directivity of the signals transmitted to the cluster to which URLLC UE  $n$  belongs is represented by  $\mathbf{w}_{m\pi_n} \in \mathbb{C}^{L \times 1}$ , and the signals transmitted to different URLLC UEs are mutually uncorrelated. In our system, we adopt maximum ratio transmission (MRT) for beamforming, where  $\mathbf{w}_{m\pi_n} = \boldsymbol{\nu}_{m\pi_n}$ .

All URLLC UEs receive signals from all APs, and the received signal at URLLC UE  $n$  is expressed as  $y_n = \sum_{m=1}^M \sum_{n'=1}^N \sqrt{p_{n'}} \mathbf{h}_{mn}^H \boldsymbol{\nu}_{m\pi_{n'}} q_{n'} + n_n$ , where  $n_n \sim \mathcal{CN}(0, 1)$  represents the noise at URLLC UE  $n$ . SIC is employed to extract the desired signal. URLLC UEs within the same cluster are decoded sequentially based on their instantaneous CSI. URLLC UEs are sorted in descending order of their channel gains, given by

$$\Omega_1 \geq \Omega_2 \geq \dots \geq \Omega_N, \quad (2)$$

where  $\Omega_n = \mathbb{E} \left\{ \sum_{m=1}^M \boldsymbol{\nu}_{m\pi_n}^H \mathbf{h}_{mn} \right\} = \sum_{m=1}^M \sqrt{\theta_{mn}}, 1 \leq n \leq N$ . However, achieving a perfect SIC is infeasible due to statistical CSI knowledge limitations and pilot contamination within the cluster [16]. Therefore, the received signal after an imperfect SIC process can be expressed as

$$\begin{aligned} \tilde{y}_n = & \underbrace{\sum_{m=1}^M \sqrt{p_n} \mathbb{E} \{ \iota_{mnn} \}}_{Y_{ds}} + \underbrace{\sum_{m=1}^M \sqrt{p_n} (\iota_{mnn} - \mathbb{E} \{ \iota_{mnn} \})}_{Y_{bu}} + \underbrace{\sum_{m=1}^M \sum_{\substack{g'=1 \\ g' \neq \pi_n}}^G \sum_{n'=1}^N x_{g'n'} \sqrt{p_{n'}} \iota_{mnn'}}_{Y_{ui}} \\ & + \underbrace{\sum_{m=1}^M \sum_{n'=0}^{n-1} x_{\pi_n n'} \sqrt{p_{n'}} \iota_{mnn'}}_{Y_{ici}} + \underbrace{\sum_{m=1}^M \sum_{n'=n+1}^N x_{\pi_n n'} \sqrt{p_{n'}} (\iota_{mnn'} - \mathbb{E} \{ \mathbf{h}_{mn}^H \boldsymbol{\nu}_{m\pi_{n'}} \hat{q}_{n'} \})}_{Y_{rici}} + n_n, \end{aligned} \quad (3)$$

where  $\iota_{mnn'} = \mathbf{h}_{mn}^H \boldsymbol{\nu}_{m\pi_{n'}} q_{n'}$  and  $\hat{q}_n$  represent the estimate of  $q_n$ . The correlation between the estimated parameter  $\hat{q}_n$  and its actual value  $q_n$  can be modeled as  $q_n = c_n \hat{q}_n + e_n$ , where

$\hat{q}_n \sim \mathcal{CN}(0, 1)$ ,  $e_n \sim \mathcal{CN}(0, \sigma_{e_n}^2 / (1 + \sigma_{e_n}^2))$ , and  $c_n = 1/\sqrt{1 + \sigma_{e_n}^2}$ . Moreover,  $\hat{q}_n$  and  $e_n$  are statistically independent. Then the SINR of URLLC UE  $n$  can be expressed as

$$\gamma_n = \frac{|Y_{ds}|^2}{|Y_{ici}|^2 + |Y_{rici}|^2 + |Y_{bu}|^2 + |Y_{ui}|^2 + n_n^2}. \quad (4)$$

### C. Achievable Data Rate for URLLC UE

FBC is employed to address transmission delays caused by an infinite coding blocklength, ensuring that the stringent QoS requirements of URLLC UEs are met. However, excessively short packet transmission can result in higher decoding error probabilities. Therefore, in the finite blocklength regime, where error-free decoding is not guaranteed, Shannon capacity is not an appropriate measure to assess the maximum achievable rate of URLLC UEs. Let  $\epsilon_n$  denote the maximum decoding error probability. The maximum achievable rate for URLLC UE  $n$  can be approximated based on the short packet transmission theory presented in [23] as

$$R_n(\gamma_n) = \log_2(1 + \gamma_n) - \sqrt{\frac{V(\gamma_n)}{n_d}} Q^{-1}(\epsilon_n) \log_2 e, \quad (5)$$

where  $Q^{-1}(\epsilon_n)$  represents the inverse of the Gaussian Q-function,  $V(\gamma_n)$  is the channel dispersion defined as  $V(\gamma_n) = 1 - (1 + \gamma_n)^{-2}$ , and  $n_d$  is the coding blocklength. As  $n_d$  approaches infinity, the effect of the second term in (5) tends to zero, resembling the behavior of Shannon capacity.

The ergodic data rate for URLLC UE  $n$  utilizing FBC can be represented as

$$\bar{R}_n = \mathbb{E}_{\gamma_n} [\max(R_n(\gamma_n), 0)]. \quad (6)$$

This rate characterizes the average achievable rate in the presence of a certain decoding error probability. However, obtaining a closed-form expression for (6) and optimizing it presents a significant challenge. To address this challenge, we can derive the LB of (6) that captures the ergodic data rate and facilitates optimization. Define  $r_n(\frac{1}{\gamma_n}) = R_n(\gamma_n)$ , where  $r_n(x) = \log_2(1 + \frac{1}{x}) - \frac{Q^{-1}(\epsilon_n)}{\ln 2 \sqrt{n_d}} \sqrt{\frac{1+2x}{(1+x)^2}}$ . It is worth noting that  $R_n(\gamma_n)$  increases with  $\gamma_n$ , while  $r_n(\gamma_n)$  decreases with  $\gamma_n$ . To ensure  $R_n(x) > 0$ , we require inequality  $f(\frac{1}{x}) \triangleq \frac{(1+\frac{1}{x}) \log_2(1+x)}{\sqrt{1+\frac{2}{x}}} > \frac{Q^{-1}(\epsilon_n)}{\ln 2 \sqrt{n_d}}$  to hold. It is observed that the first derivative of  $f(x)$  is negative, indicating the monotonic decrease of  $f(x)$ . Thus, the domain that makes  $r(x) > 0$  is  $0 < x < f^{-1}\left(\frac{Q^{-1}(\epsilon_n)}{\ln 2 \sqrt{n_d}}\right)$  [27]. The function  $f(x)$  is decreasing and convex within this domain. Based on the aforementioned analysis and applying Jensen's inequality, the following conclusions can be drawn:

$$\hat{R}_n \triangleq R(\bar{\gamma}_n^{-1}) \leq \mathbb{E}_{\gamma_n} [R(\gamma_n)] \leq \bar{R}_n, \quad (7)$$



where  $\hat{R}_n$  is the LB of the ergodic data rate and  $\bar{\gamma}_n = \mathbb{E}_{\gamma_n} [\gamma_n^{-1}]$ . In the subsequent theorem, we derive the expression for  $\hat{R}_n$ .

**Theorem 1.** *The LB of the ergodic data rate for URLLC UE  $n$  utilizing FBC in the NOMA-aided CFmMIMO system is given by*

$$\hat{R}_n = \log_2(1 + \bar{\gamma}_n^{-1}) - \sqrt{\frac{V(\bar{\gamma}_n^{-1})}{n_d}} Q^{-1}(\epsilon_n) \log_2 e, \quad (8)$$

where  $\bar{\gamma}_n$  is given by

$$\bar{\gamma}_n = \frac{\sum_{n'=1}^N p_{n'} \sum_{m=1}^M \beta_{mn} + 1}{L p_n \left( \sum_{m=1}^M \sqrt{\theta_{mn}} \right)^2} + \left( \sum_{n'=1}^{n-1} x_{\pi_n n'} \frac{p_{n'}}{p_n} + \sum_{n'=n+1}^N (2 - 2c_{n'}) x_{\pi_n n'} \frac{p_{n'}}{p_n} \right). \quad (9)$$

*Proof.* Please refer to Appendix A. □

#### D. Problem Formation

To fully leverage the potential of NOMA-assisted CFmMIMO system in supporting URLLC, we perform a joint optimization of power allocation and UE clustering to maximize the ASR. This optimization problem can be formulated as follows:

$$\max_{\mathbf{p}, \mathbf{X}} \sum_{n=1}^N \hat{R}_n \quad (10)$$

$$\text{s.t. } \hat{R}_n \geq \hat{R}_n^{req}, \quad 1 \leq n \leq N, \quad (10a)$$

$$0 \leq \sum_{n=1}^N p_n \leq p_{max}, \quad (10b)$$

$$\sum_{g=1}^G x_{gn} = 1, \quad x_{gn} \in \{0, 1\}, \quad 1 \leq n \leq N, \quad (10c)$$

$$(8), (9), \quad (10d)$$

where  $\hat{R}_n^{req}$  and  $p_{max}$  represent the minimum rate requirement for URLLC UE  $n$  and maximum transmit power of each AP. Constraint (10a) ensures that each URLLC UE meets its minimum data rate requirement, constraint (10b) limits the maximum transmission power of each AP, and constraint (10c) ensures that each URLLC UE is allocated to only one cluster.

### III. PROBLEM ANALYSIS AND SOLUTION

To address this challenging mixed-integer non-linear programming (MINLP) problem, we propose a tractable algorithm that utilizes alternating optimization to solve for  $\mathbf{p}$  and  $\mathbf{X}$  separately. Specifically, our approach involves decomposing the original problem, which aims to maximize the ASR, into two distinct subproblems: DL power allocation with fixed UE clustering and UE clustering matrix design with fixed power allocation. Through iterative optimization, we observe an augmented global ASR and eventual convergence of the original problem towards its optimal solution, attributed to the OF being upper-bounded within the feasible set. In the subsequent sections, we provide a comprehensive exposition of the optimization process.

#### A. DL power allocation based on SCA

When the UE clustering matrix is fixed, the optimization problem for DL power allocation can be expressed as

$$\max_{\mathbf{p}} \sum_{n=1}^N \ln(1 + \hat{\gamma}_n^{-1}) - a_n M(\hat{\gamma}_n^{-1}) \quad (11)$$

$$\text{s.t. } (9), (10a), (10b), \quad (11a)$$

where  $a_n = \frac{Q^{-1}(\epsilon_n)}{\sqrt{n_d}}$  and  $M(\hat{\gamma}_n^{-1}) = \sqrt{1 - \frac{1}{(1 + \hat{\gamma}_n^{-1})^2}}$ . The OF of Problem 11 is non-convex due to the presence of  $M(\hat{\gamma}_n^{-1})$ , and hence SCA is utilized to approximate  $M(\hat{\gamma}_n^{-1})$  with a logarithmic function [27], as demonstrated in the following lemma.

**Lemma 1.** *For any given  $x_0 \geq 0$ , the following inequality holds*

$$M(x) = \sqrt{1 - \frac{1}{(1+x)^2}} \leq \rho \ln(x+1) + \chi \triangleq M_0(x), \quad \forall x \geq 0, \quad (12)$$

where  $\rho$  and  $\chi$  are given by

$$\rho = \frac{1+x_0}{\sqrt{x_0^2+2x_0}} - \frac{\sqrt{x_0^2+2x_0}}{1+x_0}, \quad \chi = \sqrt{1 - \frac{1}{(1+x_0)^2}} - \rho \ln(x_0). \quad (13)$$

In addition, we have:

$$M(x_0) = M_0(x_0), \quad M'(x_0) = M'_0(x_0). \quad (14)$$

which means that the approximation  $M_0(x)$  is tight at  $x = x_0$ .

*Proof.* By substituting the expressions of  $\rho$  and  $\chi$  in (13) into (12), the equalities in (14) can be established. The subsequent focus is on proving Inequality (12).

Define  $H(x) = M_0(x) - M(x)$ , where  $H(x_0) = 0$  for some  $x_0 > 0$ . Upon differentiating  $H(x)$  with respect to  $x$ , we obtain its first-order derivative

$$H'(x) = \frac{\sqrt{x^2 + 2x}(1+x) - \sqrt{x_0^2 + 2x_0}(1+x_0)}{\sqrt{x_0^2 + 2x_0}(1+x_0)\sqrt{x^2 + 2x}(1+x)^2}. \quad (15)$$

Since  $x$  and  $x_0$  are both positive, the sign of  $H'(x)$  depends solely on the numerator. Hence, when  $0 \leq x \leq x_0$ , we have  $H'(x) \leq 0$ , and when  $x \geq x_0$ , we have  $H'(x) \geq 0$ . This implies that  $H(x)$  is monotonically decreasing for  $0 \leq x \leq x_0$  and monotonically increasing for  $x \geq x_0$ . Since  $H(x_0) = 0$ , we can conclude that  $H(x) \geq 0$  for all  $x \geq 0$ . Therefore, when  $x \geq 0$ , we have  $M(x) \geq M_0(x)$ , which completes the proof.  $\square$

The OF of Problem 11 is approximated based on Lemma 1, leading to the following reformulation of Problem 11:

$$\max_{\mathbf{p}, \boldsymbol{\kappa}} \prod_{n=1}^N \kappa_n^{(1-a_n\rho_n)} \quad (16)$$

$$\text{s.t. } \kappa_n \leq \hat{\gamma}_n^{-1} + 1, \quad 1 \leq n \leq N \quad (16a)$$

$$(9), (10a), (10b). \quad (16b)$$

Then we proceed to approximate the constraint (16a) to convert Problem 11 into a GP problem.

The constraint (16a) can be represent as

$$\frac{U(\mathbf{P})\kappa_n}{P_{d,n}(\mathbf{P}) + U(\mathbf{P})} \leq 1, \quad 1 \leq n \leq N, \quad (17)$$

where  $U(\mathbf{p})$  and  $P_{d,n}(\mathbf{p})$  is defined as

$$\begin{cases} P_{d,n}(\mathbf{p}) = Lp_n \left( \sum_{m=1}^M \sqrt{\theta_{mn}} \right)^2, \\ U(\mathbf{p}) = \sum_{n'=1}^N P_{I_1,n'}(\mathbf{p}) + \sum_{n'=n+1}^N P_{I_2,n'}(\mathbf{p}) + \sum_{n'=1}^{n-1} P_{I_3,n'}(\mathbf{p}) + 1. \end{cases} \quad (18)$$

In (18),  $P_{I_1,n'}(\mathbf{p}) = \sum_{m=1}^M p_{n'} \beta_{mn}$ ,  $P_{I_2,n'}(\mathbf{p}) = Lx_{\pi_n n'} p_{n'} \left( \sum_{m=1}^M \sqrt{\theta_{mn}} \right)^2$ , and  $P_{I_3,n'}(\mathbf{p}) = L(2 - 2c_{n'}) x_{\pi_n n'} p_{n'} \left( \sum_{m=1}^M \sqrt{\theta_{mn}} \right)^2$ .

We can manipulate the denominator in (17) and represent it as a product, which can be expressed as

$$\begin{aligned} P_{d,n}(\mathbf{p}) + U(\mathbf{p}) &\leq \prod_{n'=1}^N \left( \frac{P_{I_1,n'}(\mathbf{p})}{\alpha_{1,n'}} \right)^{\alpha_{1,n'}} \prod_{n' \in U_n^1} \left( \frac{P_{I_2,n'}(\mathbf{p})}{\alpha_{2,n'}} \right)^{\alpha_{2,n'}} \\ &\cdot \prod_{n' \in U_n^2} \left( \frac{P_{I_3,n'}(\mathbf{p})}{\alpha_{3,n'}} \right)^{\alpha_{3,n'}} \left( \frac{LM}{\alpha_4} \right)^{\alpha_4} \left( \frac{P_{d,n}(\mathbf{p})}{\alpha_{5,n}} \right)^{\alpha_{5,n}}, \end{aligned} \quad (19)$$

where  $U_n^1$  and  $U_n^2$  represent sets consisting of URLLC UEs in the same cluster as URLLC UE  $n$ , with a SIC ordering lower and higher than that of URLLC UE  $n$ , respectively. By substituting (19) into (17), we obtain a polynomial representation for (17), which is given as

$$U(\mathbf{p})\tilde{F}(\mathbf{p})^{-1}\kappa_n \leq 1, \quad 1 \leq n \leq N. \quad (20)$$

Based on the aforementioned analysis, we proceed to offer a comprehensive exposition of the power allocation algorithm.

In the  $i$ -th iteration, we denote the power allocation coefficients as  $\mathbf{p}^{(i)}$ , and the variables  $\boldsymbol{\kappa}^{(i)} = [\kappa_1^{(i)}, \kappa_2^{(i)}, \dots, \kappa_n^{(i)}]$ . Correspondingly, the coefficients  $\mathbf{w}^{(i)} = [w_1^{(i)}, w_2^{(i)}, \dots, w_n^{(i)}]$  and  $\boldsymbol{\alpha}^{(i)} = [\alpha_{1,n'}^{(i)}, \alpha_{2,n'}^{(i)}, \alpha_{3,n'}^{(i)}, \alpha_4^{(i)}, \alpha_{5,n}^{(i)}]$  can be calculated. Subsequently, in the  $i + 1$ -th iteration, we can obtain the LB of the OF using Lemma 1, and express the limit as a polynomial function with appropriate indentation as specified by (20). Finally, we can transform Problem 16 into a standard GP problem as follows

$$\min_{\mathbf{p}, \boldsymbol{\kappa}} \frac{1}{\prod_{n=1}^N \kappa_n^{w_n^{(i)}}} \quad (21)$$

$$\text{s.t. (9), (20), (10a), (10b).} \quad (21a)$$

Applying a logarithmic transformation of variables, we can convert the GP problem into a convex optimization problem. This transformed problem can be effectively solved using the interior-point method, enabling us to obtain a solution for Problem 21. The iterative algorithm for solving the power allocation problem with a fixed UE clustering matrix is presented in Algorithm 1, based on the analysis presented above.

Ensuring a feasible initial power allocation is crucial for the success of Algorithm 1. The failure of the algorithm can occur when a randomly generated power allocation scheme fails to satisfy the minimum rate requirement of certain URLLC UEs. To guarantee feasibility, we can determine the feasible solution  $\mathbf{p}^{(0)}$  by solving a dedicated feasibility problem, which is presented as

$$\max_{\mathbf{p}, \varphi} \varphi \quad (22)$$

---

**Algorithm 1:** SCA Based DL Power Allocation Algorithm

---

- 1 Initialize power allocation  $\{\mathbf{P}^{(0)}\}$ , coefficient  $\{\boldsymbol{\kappa}^{(0)}, \mathbf{w}^{(0)}, \boldsymbol{\alpha}^{(0)}\}$ , the OF of Problem 11  $\text{Obj}_1^{(0)}$ ; iteration number  $t=1$  and the upper bound  $T_{out}$  and error tolerance  $\xi$ ;
  - 2 **while**  $|\text{Obj}_1^{(i+1)} - \text{Obj}_1^{(i)}| / \text{Obj}_1^{(i)} \geq \xi$  and  $t \leq T_{out}$  **do**
  - 3     Solve Problem 21 with GP solver to obtain  $\{\mathbf{P}^{(i+1)}, \boldsymbol{\kappa}^{(i+1)}\}$  with given  $\{\boldsymbol{\kappa}^{(i)}, \mathbf{w}^{(i)}, \boldsymbol{\alpha}^{(i)}\}$ ;
  - 4     Update  $\{\mathbf{w}^{(i+1)}, \boldsymbol{\alpha}^{(i+1)}\}$  and calculate  $\text{Obj}_1^{(i+1)}$ .
  - 5 **end**
- 

$$\text{s.t. } P_{d,n}(\mathbf{p}) \geq \varphi + U(\mathbf{p})g_n^{-1}(\hat{R}_n^{rep}), \quad 1 \leq n \leq N, \quad (22a)$$

$$(10b). \quad (22b)$$

Finally, we analyze the convergence of Algorithm 1. In the  $i$ -th iteration, we obtain the value of  $\text{Obj}_1^{(i)}$ . After optimization in the  $i$ -th iteration, the approximation of the OF using Lemma 1 is found to be greater than  $\text{Obj}_1^{(i)}$ . Furthermore, since  $\text{Obj}_1^{(i+1)}$  is greater than its approximation, we have  $\text{Obj}_1^{(i+1)} \geq \text{Obj}_1^{(i)}$ . Besides, it is worth noting that the OF of Problem 11 has an upper bound due to the individual minimum rate requirements of each URLLC UE. Therefore, Algorithm 1 is guaranteed to converge.

### B. UE Clustering Matrix Design based on Graph Theory

When the power allocation is fixed, the problem of designing UE clustering matrix can be reformulated as a maximization problem, which can be represented as follows:

$$\max_{\mathbf{P}} \sum_{n=1}^N \hat{R}_n \quad (23)$$

$$\text{s.t. } (8), (9), (10a), (10c). \quad (23a)$$

By utilizing the principles of graph theory, the UE clustering matrix design problem can be effectively solved. Specifically, a weighted directed graph is constructed based on the OF of the Problem 23 and the clustering information of URLLC UEs. Subsequently, we employ two negative loop search algorithms to identify negative loops within the graph. To maximize the ASR, we introduce several definitions that are similar to those used in previous works, such as [28], [29].

**Definition 1.** If a set of  $K$  URLLC UEs, denoted as  $n_1, n_2, \dots, n_K$ , belongs to distinct clusters, and the clustering matrix  $\mathbf{X}$  can be transformed into  $\tilde{\mathbf{X}}$  by  $n_1 \rightarrow n_2, n_2 \rightarrow n_3, \dots, n_{K-2} \rightarrow n_{K-1}$ , while allocating URLLC UE  $K-1$  to the same cluster as URLLC UE  $K$ , and if the ASR satisfies  $\sum_{n=1}^N \hat{R}_n(\mathbf{X}) \leq \sum_{n=1}^N \hat{R}_n(\tilde{\mathbf{X}})$ , then these  $K$  URLLC UEs form a K-shift union.

To explain the notation  $n \rightarrow n'$ , assume that with clustering matrix  $\mathbf{X}$ , URLLC UE  $n$  and URLLC UE  $n'$  are placed in clusters  $g$  and  $g'$ , respectively. This implies that  $x_{gn} = 1$  and  $x_{g'n'} = 1$ . Then  $n \rightarrow n'$  means allocate URLLC UE  $n$  to cluster  $g'$  and removing URLLC UE  $n'$  from cluster  $g'$ . This implies that  $x_{gn} = 0$ ,  $x_{g'n'} = 1$ , and  $x_{g'n} = 0$ .

**Definition 2.** If a set of  $K$  URLLC UEs, denoted as  $n_1, n_2, \dots, n_K$ , belongs to distinct clusters, and the clustering matrix  $\mathbf{X}$  can be transformed into  $\tilde{\mathbf{X}}$  by  $n_1 \rightarrow n_2, n_2 \rightarrow n_3, \dots, n_K \rightarrow n_1$ , and if the ASR satisfies  $\sum_{n=1}^N \hat{R}_n(\mathbf{X}) \leq \sum_{n=1}^N \hat{R}_n(\tilde{\mathbf{X}})$ , then these  $K$  URLLC UEs form a K-exchange union.

Note that the *exchange union* and the *shift union* are different from each other. The former changes the clustering of URLLC UEs without altering the number of URLLC UEs in each cluster, while the latter modifies the number of URLLC UEs in each cluster. Based on these definitions, we provide the definition of the *all-stable solution*.

**Definition 3.** A clustering matrix  $\mathbf{X}$  is defined as an all-stable solution if there are no shift union or exchange union that can increase the ASR while satisfying all constraints in Problem 23.

Designing a UE clustering matrix that can increase the ASR of all URLLC UEs can be transformed as a search for either a *shift union* or an *exchange union*. The identification of these unions among UEs can be achieved by analyzing the variation of  $\sum_{n=1}^N \hat{R}_n(\mathbf{X})$  upon changing the UE clustering matrix  $\mathbf{X}$ . By decomposing the expression of  $\sum_{n=1}^N \hat{R}_n(\mathbf{X})$  into clusters, a rate variable can be defined as

$$\omega_g(\mathbf{X}) = \sum_{n=1}^N x_{gn} \left( \ln(1 + \hat{\gamma}_n^{-1}) - a_n \sqrt{V(\hat{\gamma}_n^{-1})} \right). \quad (24)$$

The interdependence between the ASR and  $\omega_g(\mathbf{X})$  can be expressed as  $\sum_{n=1}^N \hat{R}_n(\mathbf{X}) = \frac{1}{\ln 2} \sum_{g=1}^G \omega_g(\mathbf{X})$ . Thus, the impact of the changes in the UE clustering matrix  $\omega_g(\mathbf{X})$  is obtained.

A weight directed graph  $G(\mathcal{N}, \varepsilon; \mathbf{X})$  is constructed based on (24), where  $\mathcal{N}$  represents the set of nodes comprising the URLLC UEs, and  $\varepsilon$  denotes the set of edges connecting two URLLC

UEs belonging to different clusters. The adjacency matrix of the graph  $G(\mathcal{N}, \varepsilon; \mathbf{X})$  is denoted by  $\mathbf{Z}$ , and its elements are defined as follows for  $1 \leq i, j \leq N$ :

$$z_{ij} = \begin{cases} \omega_{\pi_j}(\mathbf{X}) - \omega_{\pi_j}(x_{\pi_j i} = 1, x_{\pi_j j} = 0, \mathbf{X}_{-i,j}), & \text{if } \pi_i \neq \pi_j \\ \infty, & \text{if } \pi_i = \pi_j \end{cases} \quad (25)$$

where  $\mathbf{X}_{-i,j}$  represents the clustering matrix of URLLC UEs excluding UEs  $i$  and  $j$ . Therefore,  $(x_{\pi_j i} = 1, x_{\pi_j j} = 0, \mathbf{X}_{-i,j})$  represents that UE  $i$  is in cluster  $\pi_j$ , URLLC UE  $j$  is not in cluster  $\pi_j$ , and the clustering matrix of URLLC UEs excluding URLLC UEs  $i$  and  $j$  is consistent with  $\mathbf{X}$ . The relationship between Problem 23 and graph  $G(\mathcal{N}, \varepsilon; \mathbf{X})$  can be described by the following lemma.

**Lemma 2.** *If the ASR  $\sum_{n=1}^N \hat{R}_n(\mathbf{X})$  can be increased by allocating URLLC UEs, denoted as  $n_1, n_2, \dots, n_K$ , to different clusters by  $n_1 \rightarrow n_2 \rightarrow \dots \rightarrow n_K \rightarrow n_1$ , then these URLLC UEs can form a negative loop  $n_1 \mapsto n_2 \mapsto \dots \mapsto n_K \mapsto n_1$  in the graph  $G(\mathcal{N}, \varepsilon; \mathbf{X})$ .*

*Proof.* Assuming that the UE clustering matrix before and after  $n_1 \rightarrow n_2 \rightarrow \dots \rightarrow n_K \rightarrow n_1$  is denoted as  $\mathbf{X}$  and  $\tilde{\mathbf{X}}$ , respectively, the difference in ASR is given by:

$$\begin{aligned} \Delta \hat{R} &= \sum_{n=1}^N \hat{R}_n(\mathbf{X}) - \sum_{n=1}^N \hat{R}_n(\tilde{\mathbf{X}}) \\ &= \sum_{n=1}^N \left( \log_2(1 + \hat{\gamma}_n^{-1}) - a_n \sqrt{V(\hat{\gamma}_n^{-1})} \log_2 e \right) - \sum_{n=1}^N \left( \log_2(1 + \hat{\gamma}_n^{-1}) - a_n \sqrt{V(\hat{\gamma}_n^{-1})} \log_2 e \right). \end{aligned} \quad (26)$$

Assuming that URLLC UEs  $n_1, n_2, \dots, n_K$  are allocated to clusters  $\pi_1, \pi_2, \dots, \pi_K$ , it can be observed from (4) that the SINR of URLLC UEs within these  $K$  clusters is affected. As a new URLLC UE enters a cluster, the ranking of URLLC UEs in that cluster is re-evaluated, causing the SINR and achievable rate of each URLLC UE to be recalculated. However, the SINR of URLLC UEs outside of these  $K$  clusters is not affected, and their achievable rate remain unchanged by  $n_1 \rightarrow n_2 \rightarrow \dots \rightarrow n_K \rightarrow n_1$ . Using (26), the relation between  $\Delta R$  and  $\sum_{k=1}^K a_{kj}$  is can be calculated as

$$\begin{aligned}
\Delta \hat{R} &= \sum_{k=1}^K \sum_{n=1}^N x_{\pi_k n} \left( \log_2(1 + \hat{\gamma}_n^{-1}) - a_n \sqrt{V(\hat{\gamma}_n^{-1})} \log_2 e \right) \\
&\quad - \sum_{k=1}^K \sum_{n=1}^N \tilde{x}_{\pi_k n} \left( \log_2(1 + \hat{\gamma}_n^{-1}) - a_n \sqrt{V(\hat{\gamma}_n^{-1})} \log_2 e \right) \\
&= \sum_{k=1}^K a_{kj}
\end{aligned} \tag{27}$$

where  $j = \text{mod}(k, K) + 1$ . Thus, the proof of Lemma 2 is concluded.  $\square$

The approach to increase the ASR by changing clusters involves identifying negative loops that contain URLLC UEs in different clusters, known as *negative differ-cluster loop*. However, a limitation of this approach is that the number of URLLC UEs in each cluster remains constant after the cluster changing process  $n_1 \rightarrow n_2 \rightarrow \dots \rightarrow n_K \rightarrow n_1$ . To overcome this limitation, we extend the weight directed graph  $G(\mathcal{N}, \varepsilon; \mathbf{X})$  to  $G(\mathcal{N}^e, \varepsilon; \mathbf{X})$  by introducing virtual URLLC UEs to each cluster. Specifically, a virtual URLLC UE, labeled as  $n_g^v$ , is added to cluster  $g$  to allow for arbitrary changes in the number of URLLC UEs in each cluster. These virtual URLLC UEs are assigned an ergodic data rate of 0 and do not receive any power allocation, nor do they participate in the sorting process. Thus, the presence of virtual URLLC UEs does not affect the achievable rate of real URLLC UEs. Modifying clustering matrix  $\mathbf{X}$  to  $\tilde{\mathbf{X}}$  by adding URLLC UE  $n_{K-1}$  to the cluster of URLLC UE  $n_K$  after  $n_1 \rightarrow n_2, \dots, n_{K-2} \rightarrow n_{K-1}$  can be achieved by  $n_1 \rightarrow n_2, \dots, n_{K-2} \rightarrow n_{K-1}, n_{K-1} \rightarrow n_{\pi_K}^v, n_{\pi_K}^v \rightarrow n_1$ . As a result, all *shift unions* can be converted into *exchange unions*. We present the following theorem regarding the *all-stable solution*.

**Theorem 2.** *A clustering matrix  $\mathbf{X}$  is considered an all-stable solution if there are no negative differ-cluster loop that can increase the OF of Problem 23 while satisfying all the constraints.*

*Proof.* Based on Lemma 2 and the fact that all *shift unions* can be converted into *exchange unions*, we can infer that the presence of either a *shift union* or an *exchange union* among all the URLLC UEs, including the virtual ones, necessarily implies the existence of a *negative differ-cluster loop* in the graph  $G(\mathcal{N}^e, \varepsilon; \mathbf{X})$ . Therefore, if no *negative differ-cluster loop* which can increase the OF of Problem 23 exists, it follows that there are on *shift union* or *exchange union* which can increase the ASR while satisfying all the constraints. Consequently, the clustering matrix  $\mathbf{X}$  is considered an *all-stable solution*.  $\square$



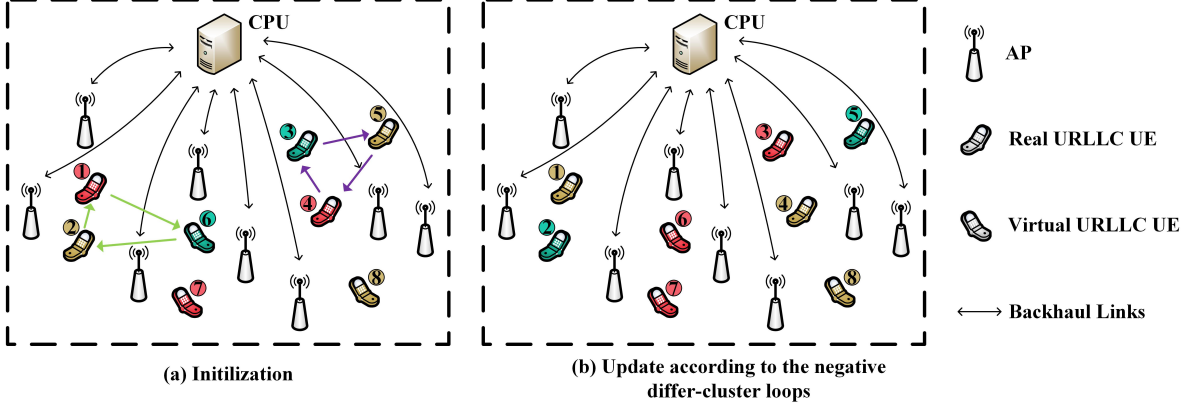


Fig. 2. Illustration of the *shift league* and *exchange league* in NOMA-aided CFmMIMO system.

Fig. 2 illustrates an example of a NOMA-aided CFmMIMO system with eight URLLC UEs, where five of them are actual URLLC UEs and three of them are virtual URLLC UEs. Our objective is to maximize the ASR by allocating these URLLC UEs to clusters. In this example, the initial assignment of the eight URLLC UEs into three clusters is depicted in Figure 2(a). The graph exhibits two *negative differ-cluster loops*:  $③ \mapsto ⑤ \mapsto ④ \mapsto ③$  and  $① \mapsto ⑥ \mapsto ② \mapsto ①$ . URLLC UEs ③, ④, and ⑤ form a *3-shift union*, while URLLC UEs ①, ⑥, and ② form a *3-exchange union*. By performing the following updates:  $③ \rightarrow ⑤$ ,  $⑤ \rightarrow ④$ ,  $④ \rightarrow ③$  or  $① \rightarrow ⑥$ ,  $⑥ \rightarrow ②$ ,  $② \rightarrow ①$ , the ASR can be increased. The modified cluster scheme after the updates is shown in Figure 2(b). It is worth noting that the initial cluster scheme is considered an *all-stable solution* if there are no *shift union* or *exchange union* among the URLLC UEs.

Based on Theorem 2, the ASR can be increased by identifying *negative differ-cluster loops* in the graph  $G(\mathcal{N}^e, \varepsilon; \mathbf{X})$  and modifying the clustering matrix until no *negative differ-cluster loop* remains in the graph  $G(\mathcal{N}^e, \varepsilon; \mathbf{X})$ . To achieve this objective, we propose an algorithm based on graph theory, which is presented as Algorithm 2. In each iteration of the algorithm, we search for a *negative differ-cluster loop* that satisfies Constraint (10a), and update the UE clustering matrix accordingly until no such loops exist in the graph  $G(\mathcal{N}^e, \varepsilon; \mathbf{X})$ .

In the fourth step of Algorithm 2, we utilize two algorithms to identify *negative differ-cluster loops* [29]. The first algorithm, known as extended bellman-ford algorithm (EBFA), involves introducing a super node into the graph and connecting it to all nodes in  $\mathcal{N}$ . The bellman-ford algorithm (BFA) seeks the shortest path from the super node to all other nodes through relaxation, continuing until no further path can be relaxed. By extending BFA, the shortest path is guaranteed to ensure that two distinct URLLC UEs within the same cluster are not present in the same path during relaxation. The second algorithm is a greedy-based sub-optimal algorithm

---

**Algorithm 2:** Graph Theory Based UE Clustering Matrix Design Algorithm

---

**Input:** UE clustering matrix design problem 23, UE clustering matrix  $\mathbf{X}^{(k)}$ , Invalid loop set  $\mathcal{S} = \phi$ .

**Output:** UE clustering matrix  $\mathbf{X}^{(k+1)}$ .

```

1 repeat
2   Create graph  $G(\mathcal{N}^e, \varepsilon; \mathbf{X}^{(k)})$ ;
3   Calculate the adjacent matrix  $\mathbf{Z} = (z_{ij})_{i,j \in \mathcal{N}^e}$  of graph  $G(\mathcal{N}^e, \varepsilon; \mathbf{X}^{(k)})$  according to
      (25);
4   Search for the negative differ-cluster loop in graph  $G(\mathcal{N}^e, \varepsilon; \mathbf{X}^{(k)})$ ;
5   if Negative differ-cluster loop  $\mathcal{L}$  not in  $\mathcal{S}$  then
6     if Constraint (10a) is not satisfied when using  $\mathbf{X}^{(k+1)}$  then
7       Add  $\mathcal{L}$  to  $\mathcal{S}$ ;
8       Go back to step 4;
9     end
10    Change clustering matrix  $\mathbf{X}^{(k)}$  to  $\mathbf{X}^{(k+1)}$  according to loop  $\mathcal{L}$ ;
11    Reorder URLLC UEs in  $\mathcal{N}$  according to new clustering matrix  $\mathbf{X}^{(k+1)}$  by (2);
12     $\mathbf{X}^{(k)} = \mathbf{X}^{(k+1)}$ ;
13  end
14   $\mathcal{S} = \phi$ .
15 until Cannot find an appropriate negative differ-cluster loop;
```

---

(GSA), which identifies the smallest edge  $z_{n_1 n_2}$  in  $\mathbf{Z}$  and repeats the process until either reaching the maximum number of iteration steps or failing to locate any *negative differ-cluster loops*. To balance the accuracy and efficiency of GSA, the coefficient  $\alpha$  can be utilized to control the number of iterations.

Finally, we analyze the convergence of Algorithm 2. The number of nodes in the graph is limited by the number of URLLC UEs and clusters, resulting in a finite number of *negative differ-cluster loops* in the graph. Besides, at each iteration of Algorithm 2, the OF of Problem 23 increases, while ensuring the feasibility of the obtained UE clustering matrix for Problem 23. Therefore, Algorithm 2 will terminate after a finite number of iterations, eventually producing a solution without any *negative differ-cluster loops*, referred to as an *all-stable solution*. Consequently, the convergence of Algorithm 2 is guaranteed.

### C. Globe ASR Maximization

The proposed algorithm for maximizing the global ASR, which integrates power allocation and UE clustering matrix design, is presented as Algorithm 3 for the original Problem 10. As discussed earlier in this section, the algorithm iteratively and alternately solves for  $\mathbf{p}$  and  $\mathbf{X}$  until a stable optimal ASR, referred to as the convergence value, is attained.

---

**Algorithm 3:** Two-Step Alternating Optimization based Global ASR Maximization

---

Algorithm

---

**Input:**  $\mathbf{p}$ ,  $\mathbf{X}$ ,  $M$ ,  $N$ ,  $G$ ,  $L$ ,  $\beta$ , error tolerance  $\xi$ , iteration number  $t = 1$  and the upper bound  $T_{out}$ ; a feasible solution  $\mathbf{p}^{(0)}$  and  $\mathbf{X}^{(0)}$  of Problem 10;

**Output:** The optimal  $\mathbf{p}^{(t)}$  and  $\mathbf{X}^{(t)}$ ;

```

1 repeat
2   obtain  $\mathbf{p}^{(t)}$  with fixed  $\mathbf{X}^{(t-1)}$  by using Algorithm 1;
3   update  $\mathbf{X}^{(t)}$  with fixed  $\mathbf{p}^{(t)}$  by using Algorithm 2;
4   set  $t = t + 1$ ;
5 until  $|\text{Obj}^{(t)} - \text{Obj}^{(t-1)}| \leq \xi$  or  $t \geq T_{out}$ ;;

```

---

**Computational Complexity Analysis:** The SDPT3 optimizer of CVX is employed to solve GP Problem 21, resulting in a complexity of  $O((2N)^3)$  with  $2N$  optimization variables. Assuming that steps 2-5 in Algorithm 1 iterate  $\tau_1$  times, the computational complexity of SPA can be expressed as  $O(\tau_1(2N)^3)$ . The computational complexity of GSA is  $O(G(G+N)^2)$ , hence the computational complexity of Algorithm 2 is  $O(\tau_2 G(G+N)^2)$  assuming GSA iterates  $\tau_2$  times. If Algorithm 3 iterates  $\tau$  times, its computational complexity can be approximated as  $O(\tau(\tau_1(2N)^3 + \tau_2 G(G+N)^2))$ .

## IV. NUMERICAL SIMULATION AND DISCUSSION

In this section, extensive simulation results validate the effectiveness of our proposed algorithms. We begin by simulating and verifying the convergence of our algorithms. Subsequently, Monte Carlo simulations are conducted to demonstrate the close approximation of the LB of the ASR to actual results. Finally, we compare the performance of the proposed algorithms with benchmark algorithms across various scenarios.

### A. Simulation Setup and Comparison Algorithms

In our simulations, we consider a randomly distributed system of APs and URLLC UEs within a rectangular area of  $1\text{km} \times 1\text{km}$ . The large-scale fading coefficient, which incorporates path loss and shadowing effects, is denoted as  $\beta_{mn} = PL_{mn} + z_{mn}$ , where  $PL_{mn}$  represents the path loss component and  $z_{mn} \sim \mathcal{CN}(0, \delta_{sh}^2)$  represents the shadowing component following a complex Gaussian distribution with zero mean and variance  $\delta_{sh}^2$ . We employ a three-slope model proposed in [10] to characterize the path loss, using the same parameter settings as in that work. Note that the length of the pilot signal is set to  $G$  to mitigate interference between clusters.

To validate the effectiveness of our proposed algorithm (S-EBFA, S-GSA), we compare their performance against the following benchmark algorithms:

- **Gale-Shapley:** In Gale-Shapley algorithm [30], each URLLC UE prefers the cluster which has less intra-cluster interference and each cluster prefer the URLLC UE which has the smaller large-scale fading coefficient. Note that the number of URLLC UEs in each cluster is not exceed  $\lceil \frac{N}{G} \rceil$ .
- **Hungarian:** URLLC UEs are allocated in different clusters by Hungarian algorithm [31], which is a common algorithm to solve the maximum matching problem of borderless weight bipartite graph. Note that the number of URLLC UEs in each cluster is not exceed  $\lceil \frac{N}{G} \rceil$ .
- **BRPA:** Basic random URLLC UE clustering without power allocation optimization algorithm (BRPA) randomly divide URLLC UEs into different clusters and only pre allocates power without any optimization.

### B. Convergence Analysis

To assess the convergence performance of our proposed algorithms, we investigate the convergence of S-EBFA and S-GSA under varying numbers of URLLC UEs, as shown in Fig. 3 and 4, respectively. We consider a scenario where there are  $M = 50$  APs, each equipped with  $L = 12$  antennas. The number of clusters is set as  $G = N/2$ . The DL data transmission length is fixed at  $n_d = 200$ , and the decoding error probability is set to  $\epsilon = 10^{-6}$ . The minimum transmission rate is restricted to 2 Mbps, while the maximum DL transmission power is set to 23 dBm. The pilot power is maintained at 20 dBm, and the SIC coefficient is assumed to be imperfect with a value of  $c = 0.5$ . Note that the parameter  $\alpha$  for S-GSA is set to 10. The results demonstrate that both algorithms exhibit rapid convergence, highlighting the low complexity and effectiveness of our proposed algorithms.

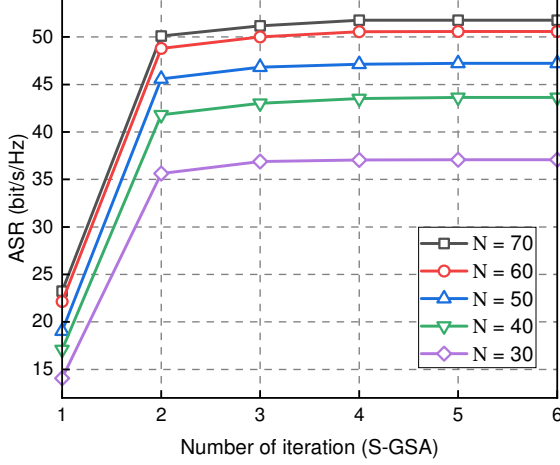


Fig. 3. Convergence of S-GSA vs. number of URLLC UEs.

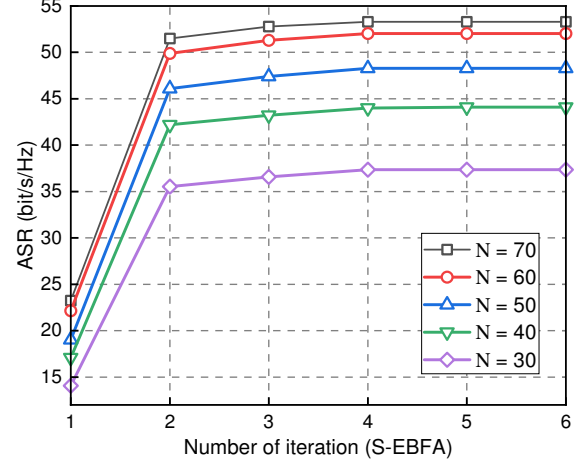


Fig. 4. Convergence of S-EBFA vs. number of URLLC UEs.

### C. Performance Analysis

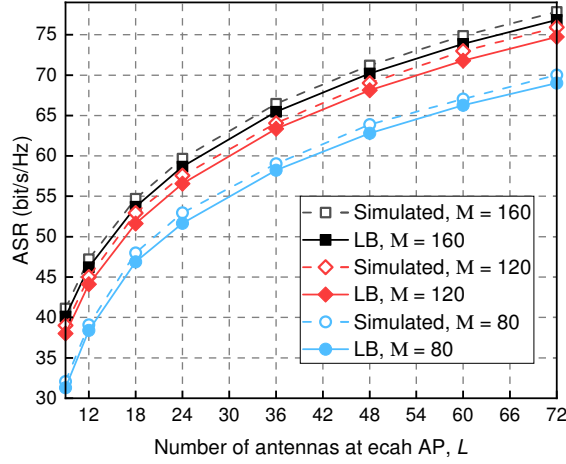


Fig. 5. Tightness of derived data rate LB vs. number of APs.

To evaluate the accuracy of the LB derived in Theorem 1, we conducted Monte Carlo simulations by generating random channels one million times and averaging the results. Figure 5 illustrates that the derived LB exhibits high precision when compared to the simulation result across various numbers of APs.

We evaluate the ASR of both our proposed algorithms and benchmark algorithms under different numbers of URLLC UEs, as illustrated in Fig. 6. Specifically, we consider a range of URLLC UEs from 20 to 90, while keeping the experimental parameter settings consistent with those outlined in Section IV-B. We observe an initial increase in the ASR as the number of URLLC UEs increases, reaching its peak at  $N = 70$ . This trend can be attributed to the strong correlation between the ASR and the number of URLLC UEs. However, the ASR subsequently

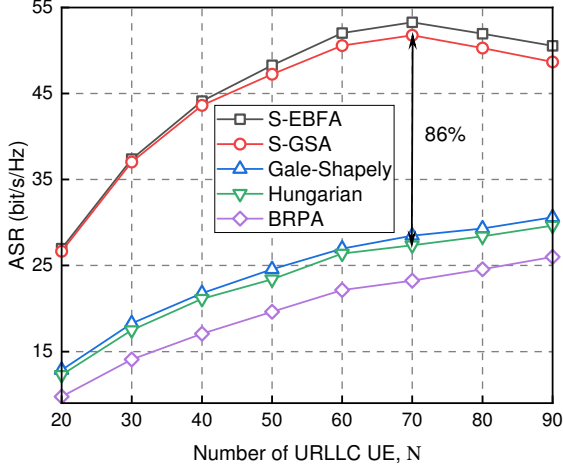


Fig. 6. ASR vs. number of URLLC UEs.

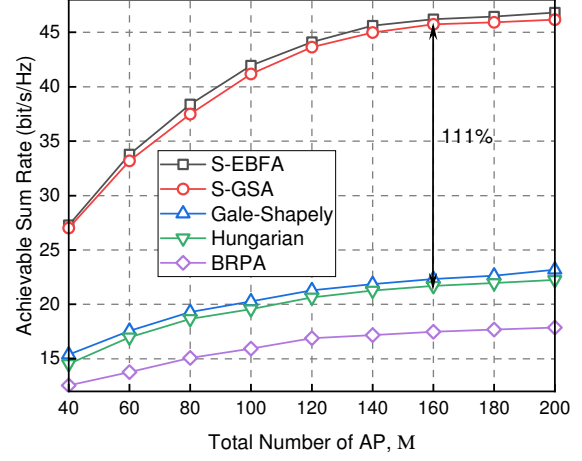


Fig. 7. ASR vs. number of APs.

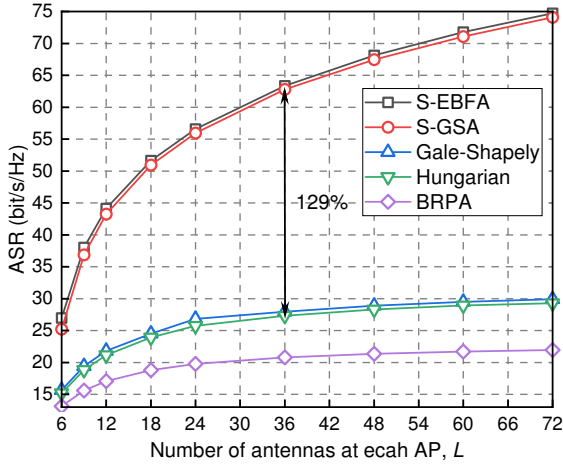


Fig. 8. ASR vs. number of antennas each AP.

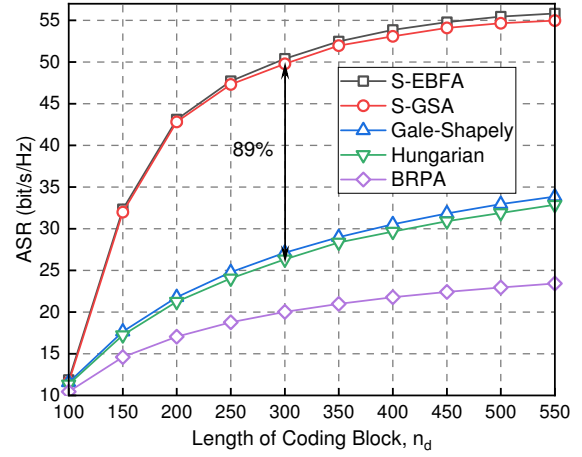


Fig. 9. ASR vs. length of blocklength.

decreases as the number of URLLC UEs increases. This phenomenon can be attributed to the increase in inter-cluster interference with the rise of URLLC UEs, leading to a more significant impact of  $P_{I1}$  than the number of URLLC UEs on the ASR, as indicated in (4). Therefore, in order to achieve the maximum sum rate, careful control of the number of URLLC UEs is necessary during actual deployment. Furthermore, our jointly optimized algorithms consistently outperform benchmark algorithms, irrespective of the number of URLLC UEs. This result is not surprising, given that our algorithm incorporates joint optimization of power allocation and UE clustering. Specifically, at  $N = 70$ , the ASR of algorithm S-GSA reaches 51 bit/s/Hz, surpassing the performance of the BRPA by 111% and the Hungarian by 86%. While the difference between S-EBFA and S-GSA is minimal, the former entails significantly higher computational complexity compared to the latter. This makes S-GSA highly effective for practical implementation.

We evaluate the performance of the proposed algorithms and other benchmark algorithms

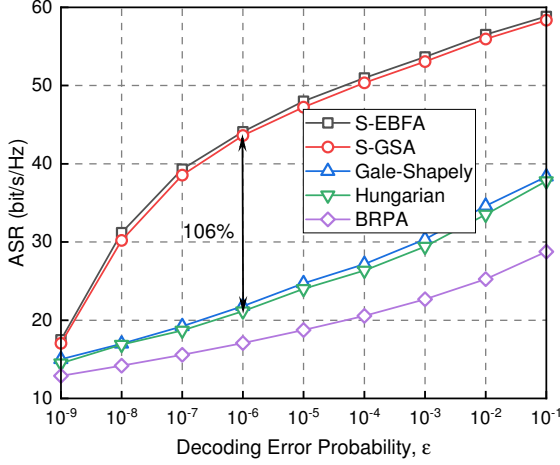


Fig. 10. ASR vs. decoding error probability.

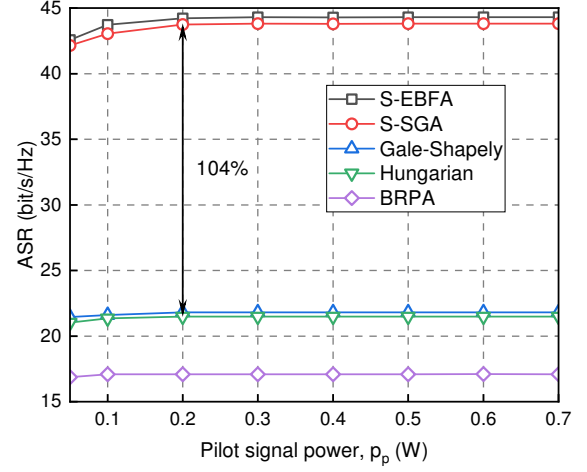


Fig. 11. ASR vs. pilot signal power.

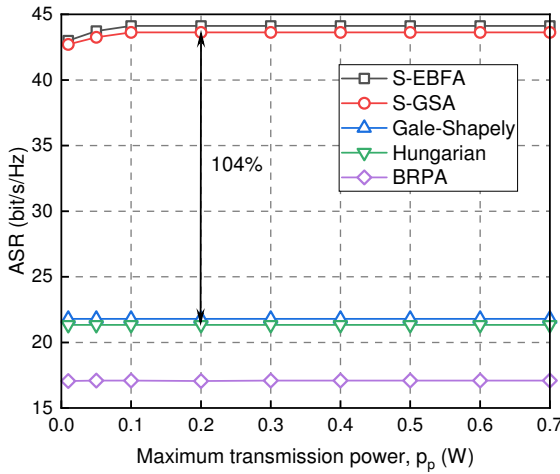


Fig. 12. ASR vs. maximum transmit power.

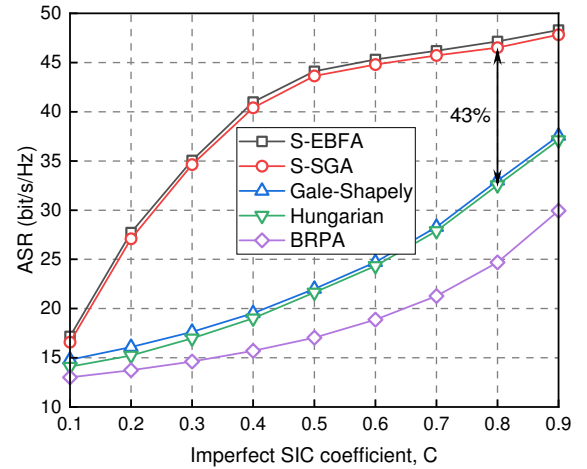


Fig. 13. ASR vs. imperfect SIC coefficient.

under varying number of APs, as illustrated in Fig. 7. The number of APs ranges from 40 to 200, while the number of URLLC UEs remains constant at 40. It is observed that the ASR increases with the increase in the number of APs. This can be attributed to the fact that the inter-cluster interference increases linearly with the number of APs, whereas the desired signal and intra-cluster interference increase with the square of the number of APs, resulting in a relatively weaker influence of inter-cluster interference as the number of APs grows. When the number of URLLC UEs is large, the ASR stabilizes as it is primarily determined by the desired signal and intra-cluster interference, while the inter-cluster interference, which grows linearly, becomes negligible in comparison. The ASR exhibits slow growth when  $M = 160$ . Therefore, selecting an optimal number of APs is crucial for ensuring QoS while minimizing power consumption, considering other system parameters. Notably, when the number of APs is  $N = 160$ , our proposed S-GSA outperforms existing algorithms such as BRPA and Hungarian



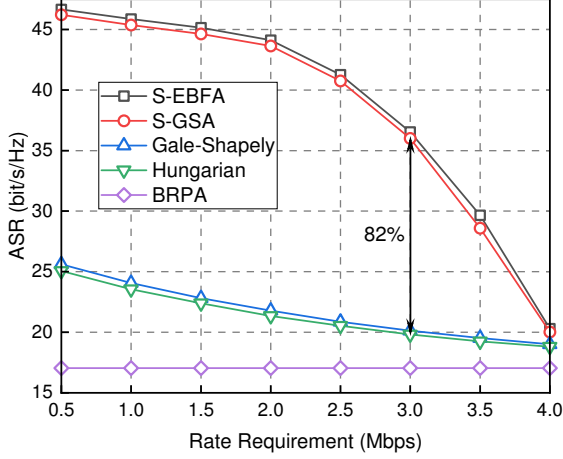


Fig. 14. ASR vs. maximum transmit power.

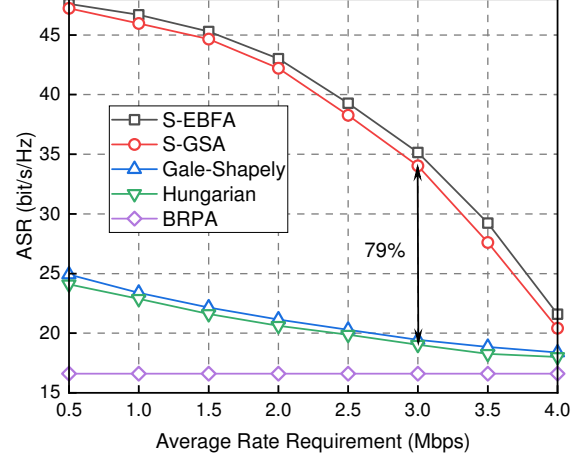


Fig. 15. ASR vs. average rate requirement.

by 162% and 111% respectively, resulting in an ASR of 46 bit/s/Hz.

We evaluate the ASR of the proposed algorithms and compare them with benchmark algorithms for different numbers of antennas at each AP, as illustrated in Fig. 8. We vary the number of antennas from 6 to 72 while fixing the number of URLLC UEs at 40. The results indicate that the ASR increases with the number of antennas at the AP. According to (4),  $P_{I1}$  and noise are unaffected by the number of antennas, while  $P_d$ ,  $P_{I1}$ , and  $P_{I2}$  increase linearly with the number of antennas, resulting in an increase in the SINR. As the number of antennas increases,  $P_{I1}$  becomes smaller than  $P_d$ , and the SINR of URLLC UEs is gradually determined by URLLC UEs in the same cluster, causing the ASR to grow more slowly and eventually stabilize. When the number of antennas is  $L = 36$ , the proposed S-GSA achieves an ASR of 63 bit/s/Hz, which is 202% and 129% higher than the BRPA and Hungarian, respectively.

The effect of the DL coding blocklength on the ASR is evaluated under different algorithms, as shown in Fig. 9. It is observed that the ASR increases as the length of the coding block increases from 100 to 550. The length of the coding block has two main effects on performance. Firstly, according to (5), the achievable rate increases with longer coding blocklength. When the coding blocklength approaches infinity, the achievable data rate will converge to the Shannon rate. Secondly, under the same SINR, the achievable data rate increases with the blocklength, making it easier to satisfy Constraint (10a). This provides more flexibility in power allocation and UE clustering, resulting in an increase in the ASR. Specifically, when the block length  $n_d = 300$ , the proposed S-GSA achieves an ASR of 50 bit/s/Hz, which is 146% higher than the BRPA and 89% higher than the Hungarian.

In Fig. 10, we evaluate the influence of the maximum decoding error probability on the



ASR with different algorithms. As illustrated, the ASR increases as the decoding error probability increases. When the maximum decoding error probability is 0.5, the achievable data rate asymptotically converges to the Shannon rate, exhibiting a similar trend to that of the coding blocklength. As the maximum decoding error probability increases, it becomes easier to meet the minimum rate requirement, thereby facilitating the growth of the ASR. When the decoding error probability  $\epsilon = 10^{-6}$ , the proposed S-GSA achieves an ASR of 44 bit/s/Hz, which is 155% and 106% higher than the ASRs of the BRPA and Hungarian, respectively.

The pilot power plays a critical role in determining the accuracy of channel estimation during UL training, as expressed in (1). A higher pilot power leads to a reduced influence of noise on the estimation accuracy. Fig. 11 shows that the ASR is hardly affected by the pilot power once it exceeds 0.1 W. This is because when the pilot power is sufficiently high, the noise can be neglected. When the pilot power is set to 0.2 W, S-GSA achieves a sum achievable rate of 44 bit/s/Hz, which is 156% and 104% higher than BRPA and Hungarian, respectively.

The increase in transmission power indirectly mitigates the effects of noise on the DL data transmission, aligning with the role of pilot power as illustrated in Eq. (4). However, excessive transmission power does not yield significant improvements in achievable rates, as depicted in Fig. 12. This suggests that a small and optimal DL power is adequate for minimizing the impact of noise. For example, when the maximum transmission power is set to  $p_d = 0.2$  W, S-GSA achieves a ASR of 44 bit/s/Hz, which represents a 156% improvement over BRPA and a 104% improvement over Hungarian.

We evaluate the ASR of the proposed algorithms and benchmark algorithms with varying imperfect SIC coefficients, as shown in Fig. 13. The ASR increases with an increase in the imperfect SIC coefficient. The coefficient primarily affects  $P_{I3}$  according to Eq. 4. To meet the minimum rate requirements when the coefficient is close to 0 and the SINR is low, there are limited power allocation and UE clustering schemes available. Therefore, the performance of the proposed algorithms does not differ significantly from that of benchmark algorithms. However, when the coefficient approaches 1, the change in  $P_{I3}$  has a greater impact on the SINR, resulting in a larger change in the ASR. When the imperfect SIC coefficient is set to  $C = 0.8$ , the ASR of algorithm S-GSA is 47 bit/s/Hz, which is 89% higher than BRPA and 43% higher than Hungarian.

We evaluate the performance of the proposed algorithms and the benchmark algorithms under varying minimum rate requirements, as illustrated in Fig. 14. With an increase in the

minimum rate requirement, the maximum achievable rate gradually decreases. The superiority of the proposed algorithms diminishes as the minimum rate requirement increases, and its final performance closely aligns with that of the benchmark algorithms. Moreover, the count of available schemes satisfying the minimum rate requirement decreases as the requirement becomes more stringent, resulting in a decrease in the ASR. Therefore, when only a few schemes can meet the QoS requirements, the performance of the proposed algorithms and the benchmark algorithms is similar. Notably, at a minimum rate requirement of  $\hat{R}^{req} = 3$  Mbps, the ASR of algorithm S-GSA is 36 bit/s/Hz, exhibiting a 106% improvement over BRPA and an 82% improvement over Hungarian.

When URLLC UEs have varying minimum rate requirements, we evaluate the performance of the proposed algorithms and the benchmark algorithms under different average rate requirements for all URLLC UEs, as illustrated in Fig. 15. As the average rate requirement increases, the maximum achievable rate of URLLC UEs gradually decreases. However, we observe that the performance of the algorithms in Fig. 15 is generally inferior to that in Fig. 14, where all URLLC UEs have the same minimum rate requirement. This can be attributed to the fact that higher rate requirements tend to impose greater limitations on power allocation and UE clustering schemes. Specifically, when the minimum rate requirement  $\hat{R}^{req}$  is set to 3 Mbps, the ASR of S-GSA is 34 bit/s/Hz, which is 104% higher than BRPA and 79% higher than Hungarian.

## V. CONCLUSION

In this paper, we have investigated the performance of the DL NOMA-aided CFmMIMO system for URLLC in terms of ASR, with consideration of FBC. Specifically, we have derived the LB for the ergodic data rate using MRT, while taking into account the effects of inter-cluster pilot contamination, inter-cluster interference, and imperfect SIC. To maximize the ASR while ensuring the minimum data rate constraint, we proposed a joint optimization framework for power allocation and UE clustering. To solve the problem efficiently, we proposed a two-step iterative algorithm where SCA is exploited to transform power allocation into a series of GPs and UE clustering is converted into finding *differ-cluster negative loop* based on graph theory. We have conducted simulations, to validate our analytical and optimization work. The results have shown that the derived LB was tight and the proposed algorithms achieved significant gains in terms of ASR compared with the benchmark algorithms under various scenarios.

Our study on supporting URLLC in the NOMA-aided CFmMIMO system remains at a preliminary theoretical level and requires further investigation. The performance of the NOMA-aided CFmMIMO system in supporting URLLC is significantly influenced by different beamforming schemes. Therefore, designing a beamforming scheme that satisfies the URLLC requirements poses considerable challenges due to the intricate nature of URLLC and necessitates thorough investigation. Furthermore, due to the unique nature of URLLC communications, the statistical QoS requirements of the NOMA-aided CFmMIMO system also necessitate further research beyond the current average QoS requirement.

## APPENDIX A

### PROOF OF THEOREM 1

According to the independence between estimated channel  $\hat{\mathbf{h}}_{mn}$  and estimate error  $\mathbf{h}_{mn} - \hat{\mathbf{h}}_{mn}$ , we derive the expression of  $|Y_{ds}|^2$  at first  $\mathbb{E}[|Y_{bu}|^2]$ ,  $\mathbb{E}[|Y_{rici}|^2]$ ,  $\mathbb{E}[|Y_{ici}|^2]$  and  $\mathbb{E}[|Y_{ui}|^2]$  as follows

$$|Y_{ds}|^2 = \left( \sum_{m=1}^M \sqrt{p_n} \mathbb{E}\{\iota_{mnn}\} \right)^2 = L p_n \left( \sum_{m=1}^M \sqrt{\theta_{mn}} \right)^2. \quad (28)$$

The expression of  $\mathbb{E}[|Y_{bu}|^2]$  is given as

$$\mathbb{E}[|Y_{bu}|^2] = \mathbb{E} \left[ \left( \sum_{m=1}^M \sqrt{p_n} (\iota_{mnn} - \mathbb{E}[\iota_{mnn}]) \right)^2 \right] = p_n \sum_{m=1}^M \beta_{mn}. \quad (29)$$

$\mathbb{E}[|Y_{ui}|^2]$  can be calculated as

$$\mathbb{E}[|Y_{ui}|^2] = \mathbb{E} \left[ \left( \sum_{m=1}^M \sum_{\substack{g'=1 \\ g' \neq \pi_n}}^G \sum_{n'=1}^N x_{g'n'} \sqrt{p_{n'}} \iota_{mnn'} \right)^2 \right] = \sum_{\substack{g'=1 \\ g' \neq \pi_n}}^G \sum_{n'=1}^N x_{g'n'} p_{n'} \sum_{m=1}^M \beta_{mn}. \quad (30)$$

Then we derive the expression of  $\mathbb{E}[|Y_{ici}|^2]$  and  $\mathbb{E}[|Y_{rici}|^2]$ .

$$\mathbb{E}[|Y_{ici}|^2] = \mathbb{E} \left[ \left( \sum_{m=1}^M \sum_{n'=0}^{n-1} x_{\pi_n n'} \sqrt{p_{n'}} \iota_{mnn'} \right)^2 \right] = \sum_{n'=0}^{n-1} x_{\pi_n n'} p_{n'} \left( \sum_{m=1}^M \beta_{mn} + L \left( \sum_{m=1}^M \sqrt{\theta_{mn}} \right)^2 \right) \quad (31)$$

$$\begin{aligned} \mathbb{E}[|Y_{rici}|^2] &= \mathbb{E} \left[ \left( \sum_{m=1}^M \sum_{n'=n+1}^N x_{\pi_n n'} \sqrt{p_{n'}} (\iota_{mnn'} - \mathbb{E}\{\mathbf{h}_{mn}^H \boldsymbol{\nu}_{m\pi_n} \hat{q}_{n'}\}) \right)^2 \right] \\ &= \sum_{n'=n+1}^N L (2 - 2c_{n'}) x_{\pi_n n'} p_{n'} \left( \sum_{m=1}^M \sqrt{\theta_{mn}} \right)^2 + \sum_{n'=n+1}^N x_{\pi_n n'} p_{n'} \sum_{m=1}^M \beta_{mn}. \end{aligned} \quad (32)$$

By substituting the above formulations into the expectation of (4), we obtain  $\hat{\gamma}_n$  in (9).

## REFERENCES

- [1] M. Bennis, M. Debbah, and H. V. Poor, “Ultrareliable and Low-Latency Wireless Communication: Tail, Risk, and Scale,” *Proc. IEEE*, vol. 106, no. 10, pp. 1834–1853, Oct. 2018.
- [2] P. Popovski, u. Stefanović, J. J. Nielsen, E. de Carvalho, M. Angjelichinoski, K. F. Trillingsgaard, and A.-S. Bana, “Wireless Access in Ultra-Reliable Low-Latency Communication (URLLC),” *IEEE Trans. Commun.*, vol. 67, no. 8, pp. 5783–5801, Aug. 2019.
- [3] D. Feng, L. Lai, J. Luo, Y. Zhong, C. Zheng, and K. Ying, “Ultra-reliable and low-latency communications: applications, opportunities and challenges,” *Sci. China Inf. Sci.*, vol. 64, pp. 1–12, Jan. 2021.
- [4] J. Navarro-Ortiz, P. Romero-Diaz, S. Sendra, P. Ameigeiras, J. J. Ramos-Munoz, and J. M. Lopez-Soler, “A Survey on 5G Usage Scenarios and Traffic Models,” *IEEE Commun. Surveys Tuts.*, vol. 22, no. 2, pp. 905–929, 2nd Quart., 2020.
- [5] P. Popovski, K. F. Trillingsgaard, O. Simeone, and G. Durisi, “5G Wireless Network Slicing for eMBB, URLLC, and mMTC: A Communication-Theoretic View,” *IEEE Access*, vol. 6, pp. 55 765–55 779, Sep. 2018.
- [6] B. Hassan, S. Baig, and M. Asif, “Key Technologies for Ultra-Reliable and Low-Latency Communication in 6G,” *IEEE Communications Standards Magazine*, vol. 5, no. 2, pp. 106–113, Jun. 2021.
- [7] J. W. Won and J. M. Ahn, “3GPP URLLC patent analysis,” *ICT Express*, vol. 7, no. 2, pp. 221–228, 2021. [Online]. Available: <https://www.sciencedirect.com/science/article/pii/S2405959520302046>
- [8] E. Nayebi, A. Ashikhmin, T. L. Marzetta, H. Yang, and B. D. Rao, “Precoding and Power Optimization in Cell-Free Massive MIMO Systems,” *IEEE Trans. Wireless Commun.*, vol. 16, no. 7, pp. 4445–4459, Jul. 2017.
- [9] J. Zhang, S. Chen, Y. Lin, J. Zheng, B. Ai, and L. Hanzo, “Cell-Free Massive MIMO: A New Next-Generation Paradigm,” *IEEE Access*, vol. 7, pp. 99 878–99 888, Jul. 2019.
- [10] H. Q. Ngo, A. Ashikhmin, H. Yang, E. G. Larsson, and T. L. Marzetta, “Cell-Free Massive MIMO Versus Small Cells,” *IEEE Trans. Wireless Commun.*, vol. 16, no. 3, pp. 1834–1850, Mar. 2017.
- [11] H. Q. Ngo, L.-N. Tran, T. Q. Duong, M. Matthaiou, and E. G. Larsson, “On the Total Energy Efficiency of Cell-Free Massive MIMO,” *IEEE Trans. Green Commun. Netw.*, vol. 2, no. 1, pp. 25–39, Mar. 2018.
- [12] Y. Li and G. A. Aruma Baduge, “NOMA-Aided Cell-Free Massive MIMO Systems,” *IEEE Wireless Commun. Lett.*, vol. 7, no. 6, pp. 950–953, Dec. 2018.
- [13] T. K. Nguyen, H. H. Nguyen, and H. D. Tuan, “Max-Min QoS Power Control in Generalized Cell-Free Massive MIMO-NOMA With Optimal Backhaul Combining,” *IEEE Trans. Veh. Technol.*, vol. 69, no. 10, pp. 10 949–10 964, Oct. 2020.
- [14] J. Zhang, J. Fan, B. Ai, and D. W. K. Ng, “NOMA-Based Cell-Free Massive MIMO Over Spatially Correlated Rician Fading Channels,” in *Proc. IEEE Int. Conf. Commun. (ICC)*, Jun. 2020, pp. 1–6.
- [15] A. A. Ohashi, D. B. d. Costa, A. L. P. Fernandes, W. Monteiro, R. Failache, A. M. Cavalcante, and J. C. W. A. Costa, “Cell-Free Massive MIMO-NOMA Systems With Imperfect SIC and Non-Reciprocal Channels,” *IEEE Wireless Commun. Lett.*, vol. 10, no. 6, pp. 1329–1333, Jun. 2021.
- [16] F. Rezaei, C. Tellambura, A. A. Tadaion, and A. R. Heidarpour, “Rate Analysis of Cell-Free Massive MIMO-NOMA With Three Linear Precoders,” *IEEE Trans. Commun.*, vol. 68, no. 6, pp. 3480–3494, Jun. 2020.
- [17] S. Kusaladharma, W. P. Zhu, W. Ajib, and G. Amarasureiya, “Achievable Rate Analysis of NOMA in Cell-Free Massive MIMO: A Stochastic Geometry Approach,” in *Proc. IEEE Int. Conf. Commun. (ICC)*, May. 2019, pp. 1–6.
- [18] S. Kusaladharma, W.-P. Zhu, W. Ajib, and G. A. A. Baduge, “Achievable Rate Characterization of NOMA-Aided Cell-Free Massive MIMO With Imperfect Successive Interference Cancellation,” *IEEE Trans. Commun.*, vol. 69, no. 5, pp. 3054–3066, May. 2021.

- [19] J. Zhang, J. Fan, J. Zhang, D. W. K. Ng, Q. Sun, and B. Ai, "Performance Analysis and Optimization of NOMA-Based Cell-Free Massive MIMO for IoT," *IEEE Internet Things J.*, vol. 9, no. 12, pp. 9625–9639, Jun. 2022.
- [20] Y. Zhang, H. Cao, M. Zhou, and L. Yang, "Spectral Efficiency Maximization for Uplink Cell-Free Massive MIMO-NOMA Networks," in *Proc. IEEE Int. Conf. Commun. Workshops (ICC Workshops)*, May. 2019, pp. 1–6.
- [21] Q. N. Le, V.-D. Nguyen, O. A. Dobre, N.-P. Nguyen, R. Zhao, and S. Chatzinotas, "Learning-Assisted User Clustering in Cell-Free Massive MIMO-NOMA Networks," *IEEE Trans. Veh. Technol.*, vol. 70, no. 12, pp. 12 872–12 887, Dec. 2021.
- [22] X.-T. Dang, M. T. P. Le, H. V. Nguyen, S. Chatzinotas, and O.-S. Shin, "Optimal User Pairing Approach for NOMA-based Cell-free Massive MIMO Systems," *IEEE Trans. Veh. Technol.*, pp. 1–15, Apr. 2022.
- [23] Y. Polyanskiy, H. V. Poor, and S. Verdú, "Channel Coding Rate in the Finite Blocklength Regime," *IEEE Trans. Inf. Theory*, vol. 56, no. 5, pp. 2307–2359, May. 2010.
- [24] G. Durisi, T. Koch, and P. Popovski, "Toward Massive, Ultrareliable, and Low-Latency Wireless Communication With Short Packets," *Proc. IEEE*, vol. 104, no. 9, pp. 1711–1726, Sep. 2016.
- [25] X. Zhao, W. Chen, and H. V. Poor, "Queue-Aware Finite-Blocklength Coding for Ultra-Reliable and Low-Latency Communications: A Cross-Layer Approach," *IEEE Trans. Wireless Commun.*, vol. 21, no. 10, pp. 8786–8802, Oct. 2022.
- [26] H. Ren, C. Pan, Y. Deng, M. El Kashlan, and A. Nallanathan, "Joint Pilot and Payload Power Allocation for Massive-MIMO-Enabled URLLC IIoT Networks," *IEEE J. Sel. Areas Commun.*, vol. 38, no. 5, pp. 816–830, Mar. 2020.
- [27] Q. Peng, H. Ren, C. Pan, N. Liu, and M. El Kashlan, "Resource Allocation for Uplink Cell-Free Massive MIMO Enabled URLLC in a Smart Factory," *IEEE Trans. Commun.*, vol. 71, no. 1, pp. 553–568, Jan. 2023.
- [28] F. Guo, H. Lu, D. Zhu, and H. Wu, "Interference-aware User Grouping Strategy in NOMA Systems with QoS Constraints," in *Proc. IEEE Conf. Comput. Commun.*, May. 2019, pp. 1378–1386.
- [29] F. Guo, H. Lu, and Z. Gu, "Joint Power and User Grouping Optimization in Cell-Free Massive MIMO Systems," *IEEE Trans. Wireless Commun.*, vol. 21, no. 2, pp. 991–1006, Feb. 2022.
- [30] W. Xu, X. Li, C.-H. Lee, M. Pan, and Z. Feng, "Joint Sensing Duration Adaptation, User Matching, and Power Allocation for Cognitive OFDM-NOMA Systems," *IEEE Trans. Wireless Commun.*, vol. 17, no. 2, pp. 1269–1282, Feb. 2018.
- [31] M. A. Sedaghat and R. R. Müller, "On User Pairing in Uplink NOMA," *IEEE Trans. Wireless Commun.*, vol. 17, no. 5, pp. 3474–3486, May. 2018.